# Sea-Level Static Testing of the Penn State Two-Dimensional Rocket-Based Combined Cycle (RBCC) Testbed

J. M. Cramer, W. M. Marshall, S. Pal and R. J. Santoro
The Pennsylvania State University
Department of Mechanical and Nuclear Engineering/
Propulsion Engineering Research Center (PERC)
University Park, PA 16802

## ABSTRACT

Twin thruster tests have been conducted with the Penn State RBCC test article operating at sea-level static conditions. Significant differences were observed in the performance characteristics for two different thruster centerline spacings. Changing the thruster spacing from 2.50 to 1.75 in. reduced the entrained air velocity (-17%) and the thrust (-7%) for tests at a thruster chamber pressure of 200 psia and MR = 8. In addition, significant differences were seen in the static pressure profiles, the Raman spectroscopy profiles, and the acoustic power spectrum for these two configurations.

## INTRODUCTION

### Programmatic Background

As part of NASA's ongoing effort to develop technology for future launch vehicles, Penn State has been performing an experimental study of the ejector mode performance of a rocket-based combined cycle (RBCC) test article. An RBCC engine operates in ejector mode during the initial stage of flight, from take-off to the transition to ramjet mode. This operating regime typically covers flight speeds from Mach 0 to 3, and dynamic pressures from 0 to 1500 psf. In this mode the rocket thrusters, which are integrated into the RBCC ramjet/scramjet air duct, fire to provide the primary propulsive force. In addition, the thrusters act as ejectors, entraining air in the duct and raising the static pressure of that air. Mixing and combusting excess fuel with this air stream augments the thrust generated by the rocket thrusters alone.[1] This thrust augmentation and the corresponding increase in specific impulse are two of the features that make an RBCC system attractive for future launch systems.

The main objective of this study is to gain insight into the physical processes involved in the mixing and combustion of the primary (rocket exhaust) and secondary (entrained air) flow streams in a representative RBCC configuration. A second objective is to develop an experimental database that can be used by CFD researchers to improve and validate their codes. The approach is to characterize these processes for single and twin thruster configurations using conventional propulsion measurements and advanced optical diagnostics. This paper highlights some of the recent measurements that have been made at sea-level static (SLS) operating conditions with the twin thrusters at different geometric spacings.

### Experiment Description

The Penn State RBCC test article is shown in Figure 1. Its two-dimensional geometry approximates a one-eighth "wedge" of an axisymmetric ejector-ramjet engine developed by

Marquardt in the mid-1960s.[1] The test article is 109 in. long from the inlet attachment flange to the duct exit plane. The flow field, including the thruster exhaust, is assumed to be uniform across the 3 in. width of the duct. For SLS testing, a linear converging inlet section, which is open to the atmosphere, is installed at the front of the duct. Downstream of the inlet section, either a single thruster is mounted on the duct centerline (Figure 1), or twin thrusters are mounted with a fixed spacing between their centerlines ($\Psi$ in Figure 2). The combined blockage area, nozzle exit area, and rocket propellant flow rates of the twin thrusters equal those values of the single thruster. Thus a direct comparison of results can be made between the single and twin thruster configurations. The constant area mixer/combustor section, which is immediately downstream of the thruster exit plane, is 5 in. high, 3 in. wide, and 35 in. long. As shown in Figure 1, all axial distances in the duct are referenced to the thruster exit plane (x = 0 in). Additional details of the duct and thruster geometry can be found in References 2 and 3.

The gaseous oxygen/gaseous hydrogen ($GO_2/GH_2$) thrusters operate at a chamber pressure of 200 psia and a mixture ratio (MR) of either 4 or 8. For stoichiometric tests (MR = 8) additional $GH_2$ is injected in the afterburner section (Figure 1).

**Previous Results and Issues**

Tests were conducted in 2000 and 2001 with the single thruster and twin thruster ($\Psi$ = 2.5 in.) configurations. In parallel to the test program, engineers at NASA/Marshall Space Flight Center performed CFD analyses of the RBCC engine at the same operating conditions.[4] Some of the significant results from those tests, and the corresponding CFD analyses, include:

1) Compared to the single thruster configuration, the twin thruster configuration showed a significant decrease in the primary/secondary mixing length in the combustor section. This effect is illustrated in Figure 3, which shows temperature profiles derived from Raman spectroscopy measurements[3] at x = 6.3 in. for both configurations. While the twin thruster profile is uniform across the duct height indicating that mixing is complete at this location, the single thruster data has a distinct jet profile. The axial static pressure profiles in Figure 4 provide another view of the mixing process for these two configurations. Mixing is considered to be complete when the pressure profile reaches a steady value in the constant area combustor. Based on this criterion, the twin thruster mixing length is ~ 6 in., while the single thruster mixing length is ~ 20 in.

2) Significantly more air was entrained in the twin thruster SLS tests than in the corresponding single thruster tests. This difference was 9% for MR = 4 and 18% for MR = 8.

3) The entrained air flow rate for the single and twin thruster tests were significantly larger than the corresponding CFD predictions (26% and 40%, respectively). The experimental values were based on a single sidewall static pressure measurement in the inlet section. An inlet velocity was calculated using this static pressure in the compressible flow equations. In order to estimate the entrained air flow rate, the assumption was made that this calculated velocity was uniform across the entire inlet area. Because of the assumptions used to estimate the experimental air flow rates, the differences between the predicted and measured values were considered to be only approximate.

4) Static pressure measurements immediately downstream of the thruster exit plane ($x > 0$ in.) had significant variation across the height of the duct. Figure 5 depicts axial static pressure profiles for $\Psi = 2.5$ in. and MR = 8. Axial profiles were measured along the top wall ($y = +2.5$ in.), the centerline of the duct ($y = 0$ in.), and the centerlines of the thrusters ($y = \pm 1.25$ in.). The area near the top wall ($A_{2,w}$) and along the duct centerline ($A_{2,c}$) are both regions where entrained air should be entering the mixing zone, but the static pressure in these two locations are quite different. At $x = 2.3$ in., the difference in static pressure between the top wall and the centerline is over 2 psid (14.5 vs. 12.2 psia). These pressure gradients in the transverse (y) dimension eventually dissipate. At $x > 8$ in., the static pressure appears to vary only in the axial (x) dimension.

5) Figure 6 presents another view of the flow field for $\Psi = 2.5$ in. and MR = 8. This figure shows the Raman-derived temperature profile at $x = 1.4$ in. The centerlines of the thrusters at $y = \pm 1.25$ in. are also shown for clarity. The peak temperature regions are not along the thruster centerlines, but rather they are bent out toward the top and bottom walls. This biasing of the primary flow streams toward the walls seems to indicate that the entrained air is more prevalent in the center region ($A_{2,c}$) than the wall regions ($A_{2,w}$).

6) Raman spectroscopy data was collected for $\Psi = 2.5$ in. and MR = 8. Individual Raman images were taken at 10 Hz with a very short exposure time (30 ns). These individual images had significant shot-to-shot variation, especially near the thruster exit plane. This variation in Raman signal strength and position appeared to be random, indicating that oscillations may be occurring in the flow field at frequencies much higher than 10 Hz.

**Current Test Series**

The primary objective of the current test series was to evaluate the effects of changing the twin thruster spacing ($\Psi$). In addition to operating at the previous spacing ($\Psi = 2.50$ in.), tests were run at $\Psi = 1.75$ in. All tests were conducted at SLS conditions, with a thruster mixture ratio of either 4 or 8.

A second objective was to develop a better understanding of the issues discussed in the previous section. In order to meet this objective, a number of instrumentation changes were made, as highlighted in Figure 2. These changes included:

1) A pitot static probe was installed in the inlet section of the duct to provide a more reliable measurement of air inlet velocity. Measurements were made approximately 2 in. upstream of the thruster aerodynamic nosecones ($x = -13.65$ in.) and along the center of the duct width ($z = 0$ in.). The pitot probe was moved from $y = -2.0$ to $+2.0$ inches in 0.5 inch increments to produce a velocity profile. Measurements were made at one fixed transverse (y) location during a test. Typically, steady-state data from 3 to 5 tests were used to determine an average value of axial velocity at each location.

2) In order to develop a clearer picture of the static pressure profiles in the duct, several measurement ports were added. As illustrated in Figure 2, pressure ports were added on the top and side walls along the length of the thrusters. These static pressure ports could

be used to discern differences between the entrained air flowing through $A_{2,c}$, and the air flowing through $A_{2,w}$. In order to better characterize the transverse pressure gradients in the mixing region (Figure 5), columns of 11 static pressure ports were added along the sidewall. The columns extended from y = -2 in. to +2 in., providing a more detailed view of the transverse pressure gradients. These measurement columns could be moved along the sidewall in 0.25 in. increments, from x = 1.15 in. to 12.65 in. A two-dimensional map of the static pressure was developed by making measurements at several axial locations.

3) In an attempt to characterize oscillations in the flow field, measurement ports for high frequency pressure transducers were added in the duct sidewalls. These ports are located at x= 0, 2.4, 6.4, 13.4, and 20.4 in. (Figure 2). The transducers can be mounted along the duct centerline (y = 0 in.) or at y = ± 0.875 in.

## RESULTS & DISCUSSION

### Entrained Air Flow

The measured inlet air velocity profile for $\Psi$ = 2.50 in. and MR = 8 is shown in Figure 7. Also depicted is the corresponding velocity profile from the NASA CFD calculations. Both of these velocity profiles are relatively flat from y = -2 to +2 in. Although the accuracy of the pitot probe decreases significantly near a wall, there appears to be reasonable agreement in the shape of the measured and CFD-predicted velocity profiles in the boundary layer at the bottom of the duct. Also plotted in Figure 7 are the average of the velocity values (measured and CFD) from y = -2 to +2 in. These average velocity values were used for comparison.

A comparison of average measured velocities and the corresponding CFD predictions are shown in Table 1. There was a significant decrease in air velocity when the twin thruster spacing was changed from 2.50 to 1.75 in. This decrease was ~ 17% for tests at both MR = 4 and 8. The measured thrust data followed the same trend, with a 6-7% decrease in thrust for $\Psi$ = 1.75 in.

This decrease in air velocity was not predicted by the CFD results, which remained virtually unchanged for the two spacings. In addition, the air velocity data confirmed a significant difference between the CFD predictions and values measured with the pitot static probe. These differences were 44% for $\Psi$ = 2.50 in. and 19% for $\Psi$ = 1.75 in.

### Static Pressure Measurements

The two-dimensional static pressure map for $\Psi$ = 2.50 in. and MR = 8 is shown in Figure 8. The thruster centerlines and the vertical extent of the nozzle exit area and the nozzle body are shown for clarity in this figure. The static pressure shows significant variation across the height of the duct in the first 3-4 inches downstream of the thruster exit plane. At x ~ 5 in., the static pressure begins to approximate a one-dimensional flowfield. However, the static pressure does continue to rise beyond x = 5 in. The low pressure regions near the thruster exit plane correspond to the secondary flow areas along the duct centerline ($A_{2,c}$) and near the top and bottom walls ($A_{2,w}$). A pressure imbalance on the two sides of the thruster centerlines is evident for the first 2-3 inches of the mixing region. The inside edge of the thruster plumes are at a significantly higher

pressure than the corresponding points on the outside edge (13.9 vs. 12.7 psia). Although there is no clear explanation for how it is formed, this pressure imbalance does help explain the tendency of the thruster exhaust to be biased toward the top and bottom walls for this case as seen in Figure 6.

Figure 9 shows the corresponding static pressure map for $\Psi$ = 1.75 in. and MR = 8. Although this map only extends to x = 4.40 in., it is clear that there is much less variation in the transverse pressure profile. In addition there appears to be no significant pressure imbalance across the thruster centerlines that would tend to steer the primary flows off their centerlines. This observation is reinforced by Figure 10, which shows the normalized nitrogen Raman signal profile at x = 2.4 in. for the same case. The regions of low nitrogen signal, which indicate the location of the hot primary flow stream, are located roughly on the thruster centerlines without the wall bias seen in the data for $\Psi$ = 2.50 in.

**High Frequency Pressure Measurements**

High frequency pressure data was collected at 20 kHz at several locations in the duct. Figure 11 depicts the power spectrum for MR = 8 with the two twin thruster spacings. These measurements were made at x = 2.4 in., y = $\pm$ 0.875 in. The transducers were on the centerline of the thrusters for $\Psi$ = 1.75 in., but they were located inside the centerlines for $\Psi$ = 2.50 in.

The area under the two power spectrum curves are approximately equal– 3518 $psi^2$ for $\Psi$ = 2.50 in. and 3725 $psi^2$ for $\Psi$ = 1.75 in. The fact that these two areas are roughly equal indicates that the total acoustic power for these two flow fields are about the same. The spectral characteristics for these two configurations are very different, however. For $\Psi$ = 2.50 in., the predominant acoustic mode is at a frequency of ~ 2400 Hz, with higher harmonics at 4800, 7200, and 9600 Hz. For $\Psi$ = 1.75 in., there is a fairly broad peak at ~ 5400 Hz which is flanked by smaller, broad peaks at 4400 and 6400 Hz. The analysis of this high frequency data is ongoing, and no firm conclusions can be drawn. However, it is clear from Figure 11 that the spectral characteristics for the two thruster spacings is very different.

## SUMMARY

The RBCC test data presented in this paper indicates that the twin thruster spacing ($\Psi$) has a significant effect on the performance characteristics. The entrained air inlet velocity, thrust, static pressure profiles, and high frequency flow characteristics all indicate significant differences between $\Psi$ = 2.50 in and $\Psi$ = 1.75 in.

## REFERENCES


[1] Odegaard, E. A. and Stroup, K. E., "1966 Advanced Ramjet Concepts Program, Volume VIII- Ejector Ramjet Engine Tests- Phase I," The Marquardt Corporation, Technical Report AFAPL-TR-67-118 Volume VIII (1968).

[2] Cramer, J., Lehman, M., Pal, S., Lee, S.-Y., and Santoro, R. J., "Status Report on the Penn State RBCC Test Program," PERC 12th Annual Symposium on Propulsion, October 2000.

[3] Cramer, J. M., Greene, M., Pal, S. and Santoro, R. J., "RBCC Ejector Mode Operating Characteristics for Single and Twin Thruster Configurations," AIAA Paper 2001-3464, July 2001.

[4] West, J., Ruf, J. H., Cramer, J., Pal, S., and Santoro, R., "Computational Insight to an Experimentally Observed Change in the Mixing Characteristics of an RBCC Engine in Ejector Mode," AIAA Paper 2001-3459, July 2001.

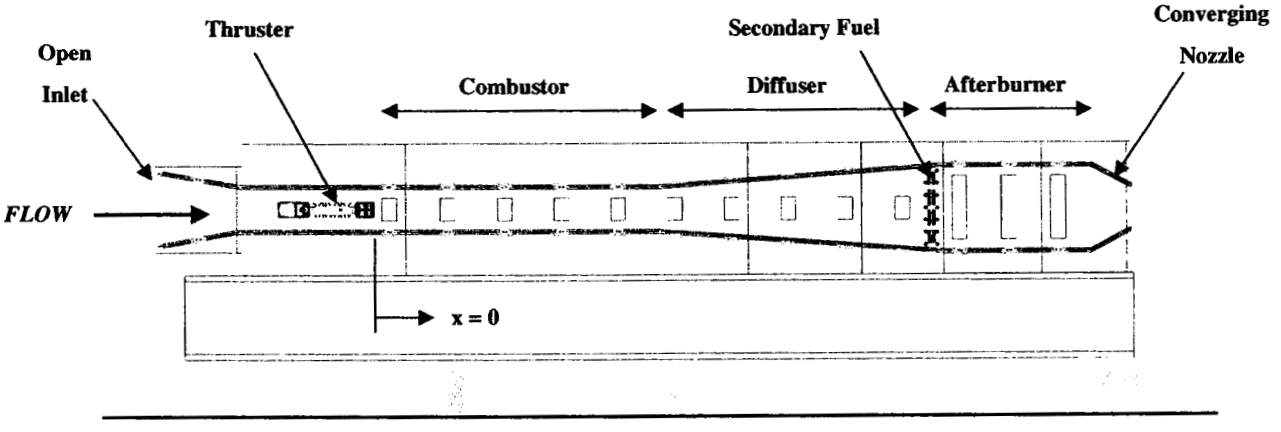


**Figure 1.** RBCC test article (single thruster, sea-level static configuration).

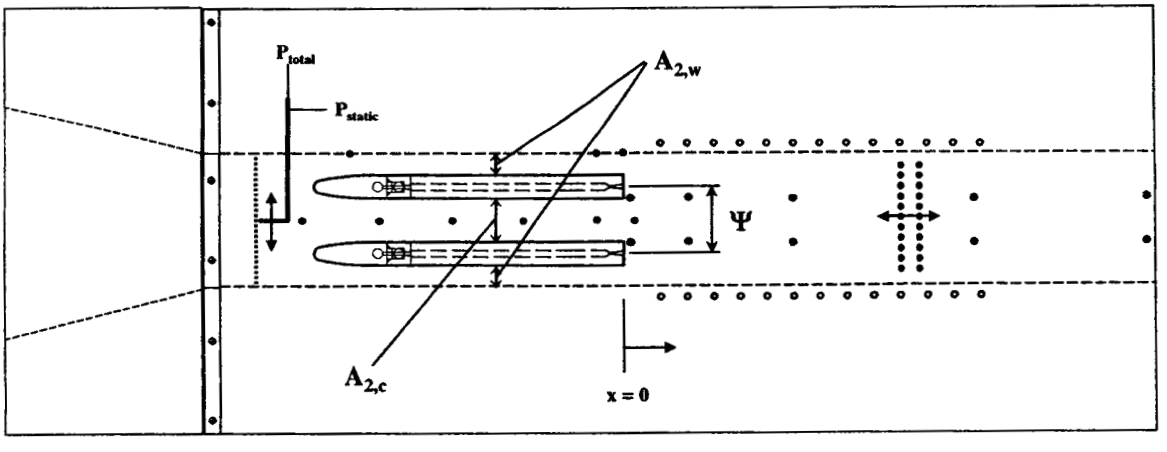


**Figure 2.** Twin thruster configuration with new instrumentation locations highlighted.

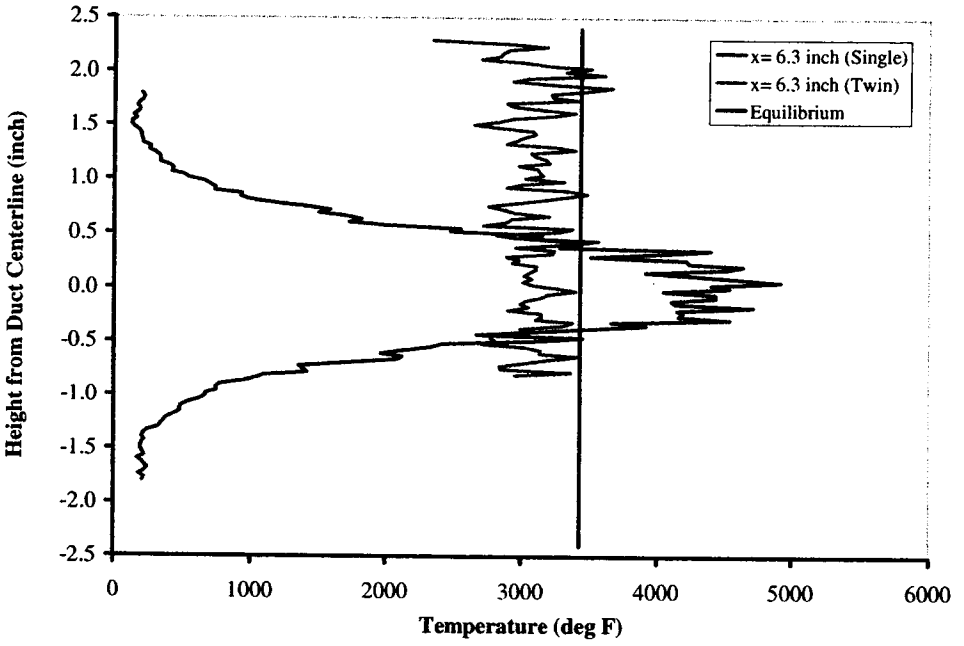


**Figure 3.** Raman-derived temperature profile for single and twin ($\Psi$= 2.5 in.) thruster configurations at x = 6.3 in., MR = 8.

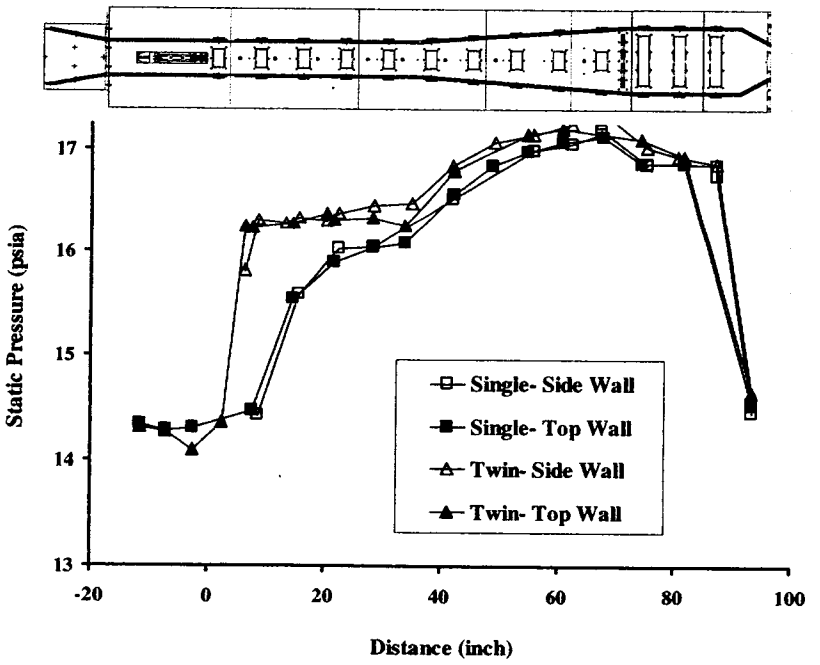


**Figure 4.** Axial static pressure profile for single thruster and twin thruster ($\Psi$ = 2.5 in.) configurations.

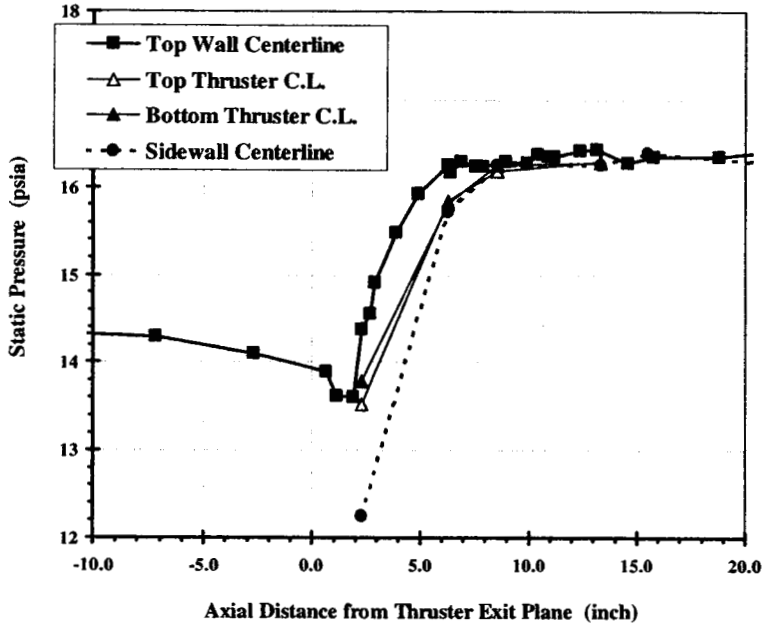


**Figure 5.** Transverse static pressure variation for twin thruster configuration ($\Psi$ = 2.5 in.).

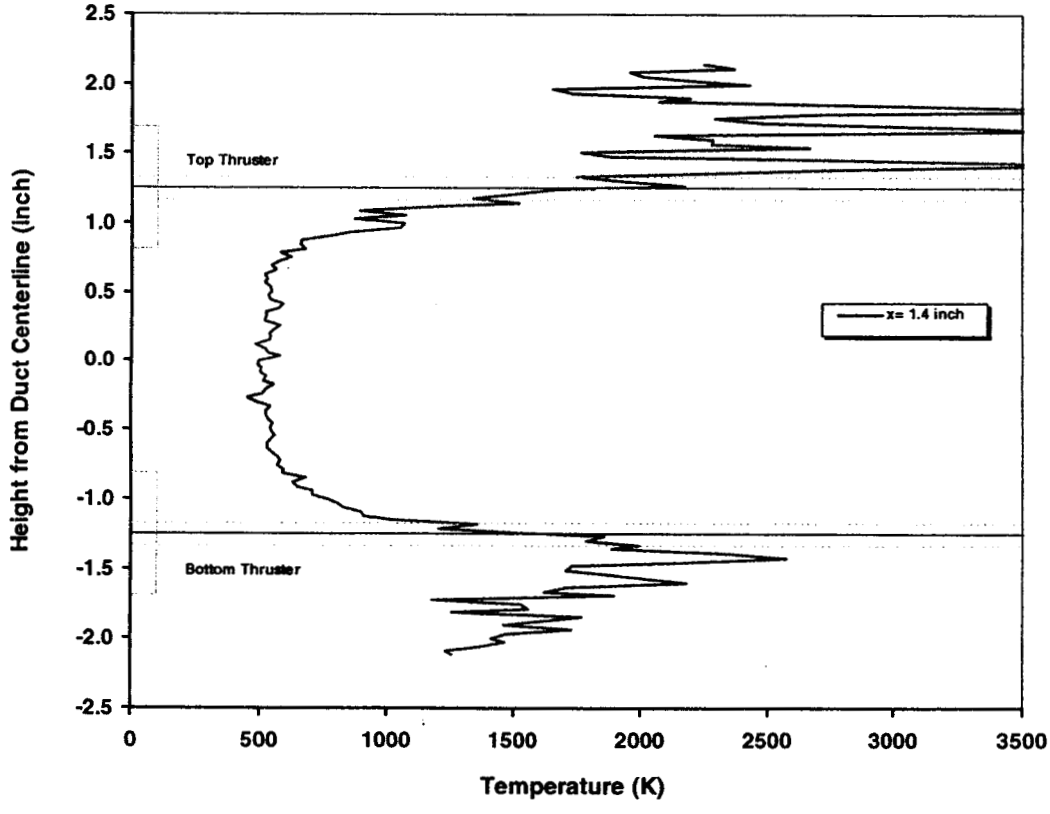


**Figure 6.** Raman-derived temperature profile for twin thruster configuration ($\Psi$ = 2.50 in., x = 1.4 in., MR = 8).

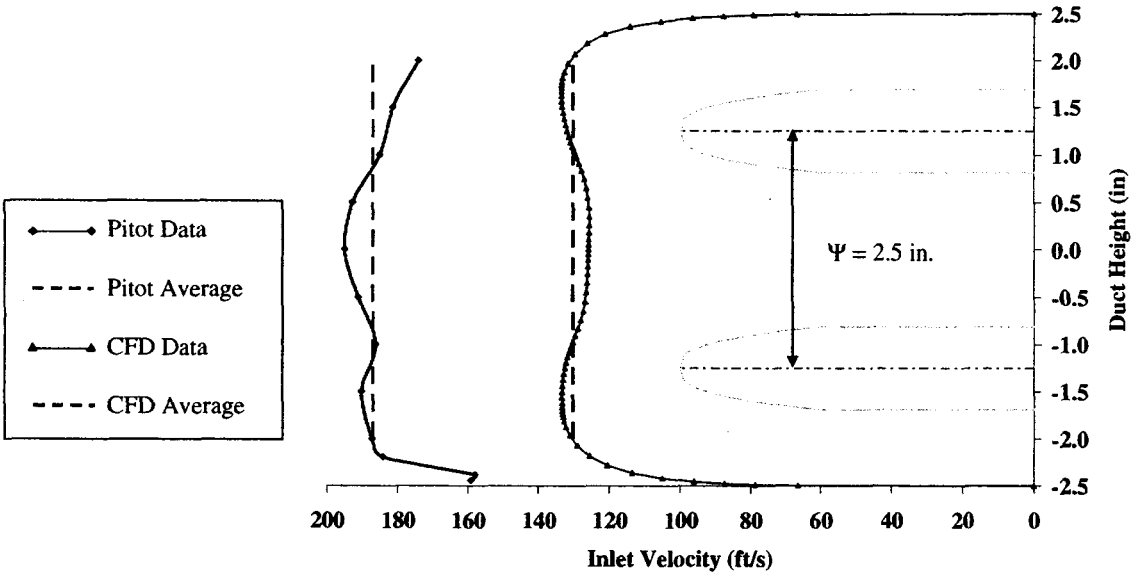


**Figure 7.** Inlet air velocity profile for twin thruster configuration (Ψ = 2.5 in., MR = 8).

| | *Case 5 (MR = 4)* | | | *Case 6 (MR = 8)* | | |
|---|---|---|---|---|---|---|
| **Thruster Configuration** | **Average Measured Air Velocity (ft/s)** | **Average CFD Air Velocity (ft/s)** | **Average Measured Thrust (lbf)** | **Average Measured Air Velocity (ft/s)** | **Average CFD Air Velocity (ft/s)** | **Average Measured Thrust (lbf)** |
| **Twin (Ψ = 2.50 in.)** | **181.5** | **N/A** | **59.6** | **187.0** | **130.3** | **71.3** |
| **Twin (Ψ = 1.75 in.)** | **151.2** | **N/A** | **56.2** | **155.0** | **129.9** | **66.3** |
| **% Change** | **-16.7** | | **-5.7** | **-17.1** | **-0.3** | **-7.0** |

**Table 1.** Inlet air velocity and measured thrust.

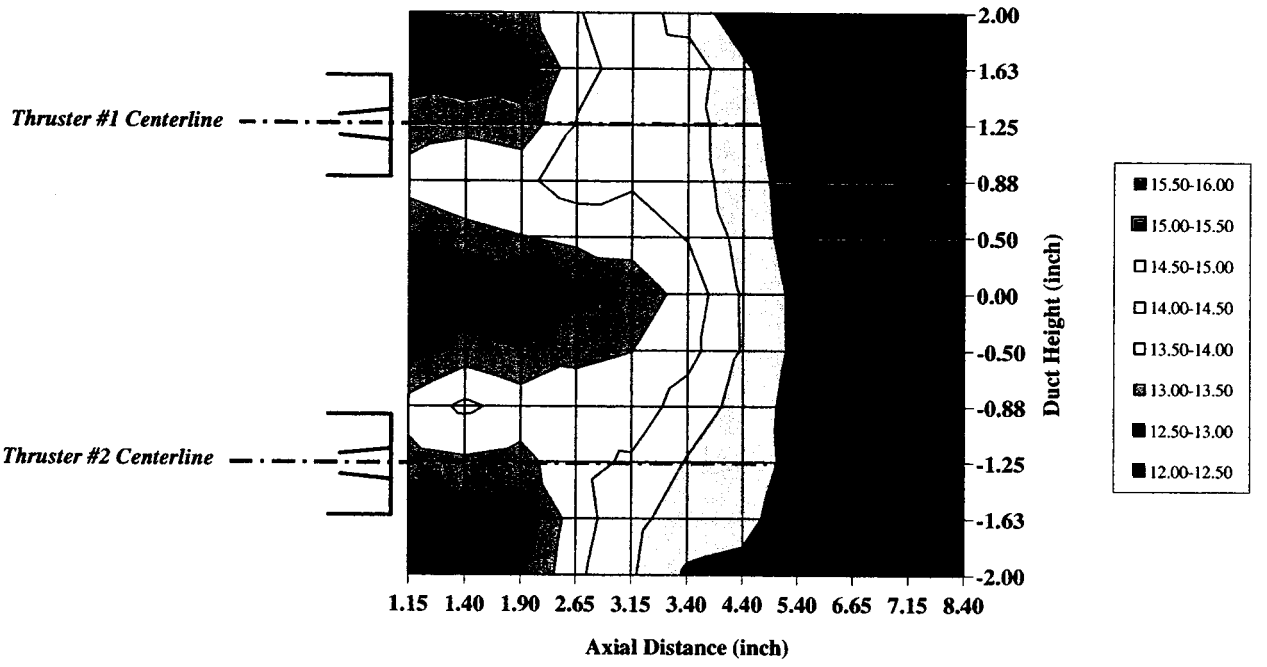


**Figure 8.** Two-dimensional static pressure maps for $\Psi = 2.50$ in., MR = 8.

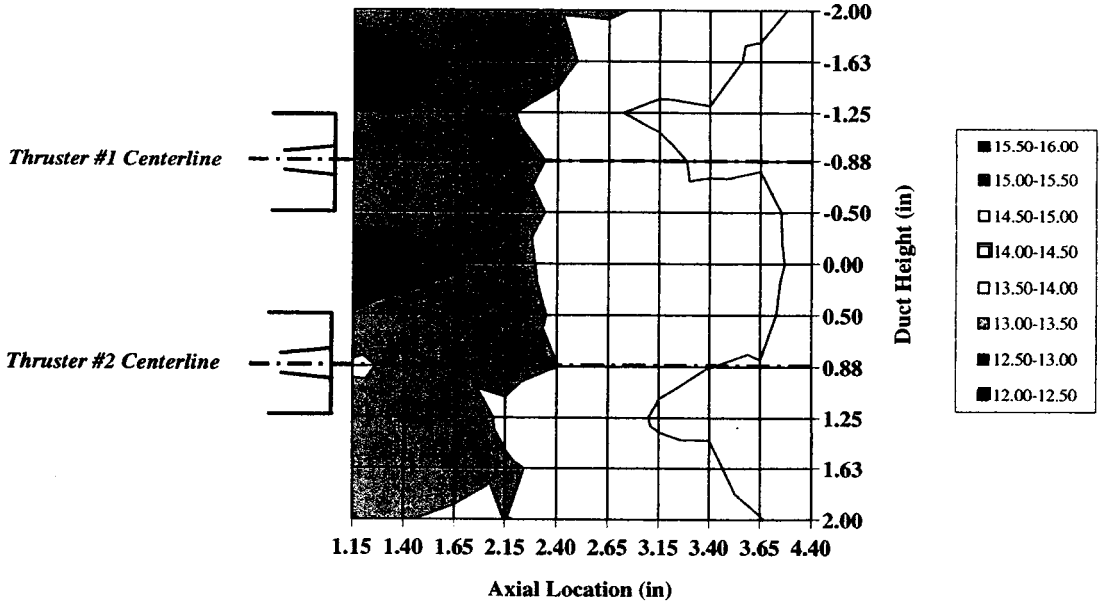


**Figure 9.** Two-dimensional static pressure maps for $\Psi = 1.75$ in., MR = 8.

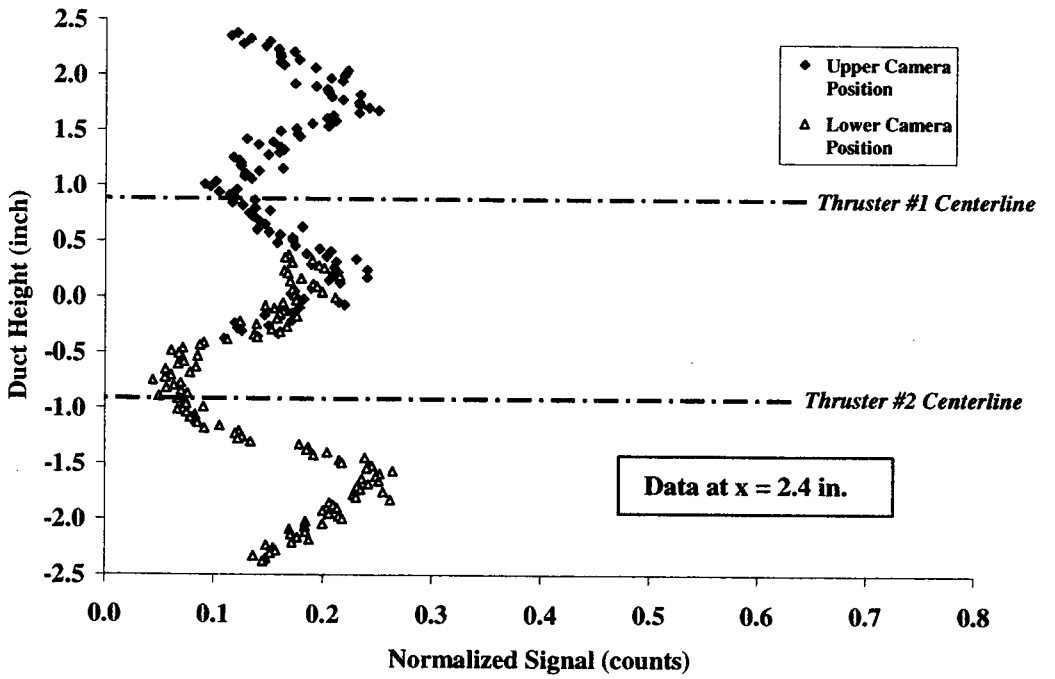


**Figure 10.** Normalized nitrogen Raman signal ($\Psi$ = 1.75 in., x = 2.4 in., MR = 8).

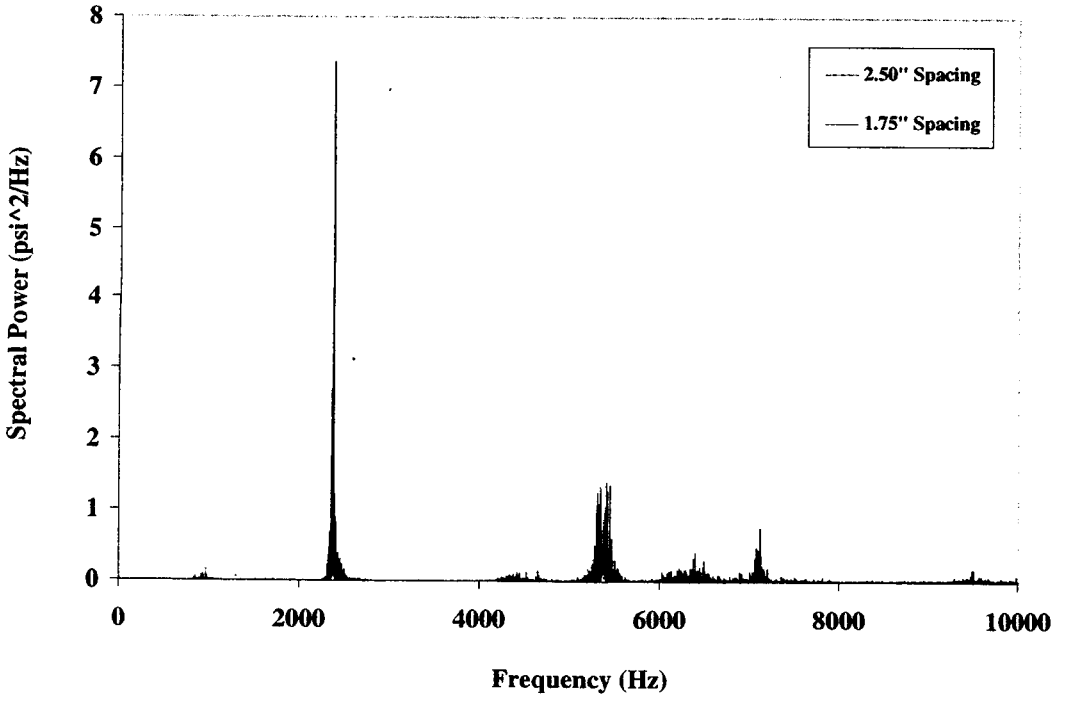


**Figure 11.** Power spectrum ($\Psi$ = 2.50 and 1.75 in., x = 2.4 in., MR = 8).